Plate Impact and Plastic Deformation by Projectiles

Major objective of this study was to investigate the transverse deformation of thin plates in the plastic range after normal impact by a blunt projectile

by P. Beynet and R. Plunkett

ABSTRACT—The problem of plastic deformation of thin plates struck by blunt projectiles but not perforated is considered. A streak camera and moiré technique were developed to measure the deflection as a function of time for the first few hundred microseconds after impact. The maximum radial strain is about three times the yield strain, the maximum tangential strain is very small. From these and other considerations it was found that there are three main regions of deformation. Since this is a traveling-wave problem, there is a radius beyond which there is no deformation. Inside of this is an annular region traversed by elastic bending waves of the Boussinesq type. Inside of this is an annular region whose dynamic behavior is governed by a membrane stress equal to the tensile yield stress and whose outer boundary travels at a wave velocity governed by the membrane equation. The inner region is a circular region of the diameter of the projectile and traveling with it. The projectile slows and comes to a stop after about 200 or 300 μsec. After this, the material unloads elastically; this elastic vibration behavior was not investigated. Both the time–displacement curve for the projectile and the displacement as a function of radius for specific times can be calculated numerically for dimensionless radius and dimensionless time for one parameter which is governed primarily by the projectile relative mass. The measured and predicted displacements agree within a few percent, except near the boundary between the plastic and the elastic region, for all times up to when elastic unloading commences.

Introduction

The elastodynamic analysis of an infinite plate subjected to a constant concentrated force impulsively applied was first made by Boussinesq in 1885[1]; he found the solution by a specific change of variable which limited him to a constant force and this gave a constant velocity of the point of impact. This solution is purely elastic and is based on Poisson plate theory neglecting membrane stresses. Goldsmith[2] put this closed-form solution into a Sneddon-type integral-equation formulation to account for the finite kinetic energy of a finite-impact mass, calculated the response numerically and verified the results experimentally within reason. Yamaishi[3] showed that, for short times, the small-deflection elastic response is given quite accurately by the coordinate transformation of Boussinesq. Duwez, Clark and Bohnenblust[4] were able to use the same transformation to predict the behavior of beams even under plastic deformation. However, all efforts to apply similar analysis to plates have failed.

Prager, Hopkins and Wang[5] have used a Poisson bending theory with associated flow rule which leads to the concept of a plastic-hinge circle traveling outward from the impact point. Many authors have investigated the behavior of a plate subject to a blast load over its whole surface and have included interaction between membrane and bending stress. A number of authors have investigated the behavior of a membrane with no bending stiffness struck by a projectile; among them are Galin[6], Rakhmatulin and Demyanov[7] and Dinca[8]. Their solutions found by integrating along four or two characteristics are presented at length by Cristescu[9].

Duffey and Key[10] use a finite-element solution and a general-purpose computer code (DEPROSS) to calculate the plastic behavior for this problem; in this case, there is no need to make any assumptions about tension or bending as such, but the stress–strain trajectories are so complicated as to be difficult to follow. This report, a condensation of a larger project[11], presents analytical and experimental evidence to show that, at least for some range of parameters, the plastic behavior depends only on the radial-in-plane membrane yield stress and involves negligible bending or shear. This result has a major influence on the penetration parameters for those configurations for which such an approximation is valid.

Experimental Methods

Moiré Displacement Fringes

The major objective of this study was to investigate the transverse deformation of thin plates in the

P. Beynet is Professor, Universite de Sherbrooke, Sherbrooke, P. Q., Can. R. Plunkett is Professor of Mechanics, Department of Aerospace Engineering and Mechanics, University of Minnesota, Minneapolis, Minn. 55455.

plastic range after normal impact by a blunt projectile. For a given projectile mass, there is a rather narrow range between that velocity just large enough to cause inelastic deformation and that large enough to cause penetration. The amount of total deformation is very sensitive to small changes in impact velocity. As a result, accurate control of the projectile velocity is important for studies of this type. For the aluminum alloys covered in this study, the velocity just to cause plastic flow is a function of the plate thickness and is about 1000 in./sec for the plates used; the maximum velocity of interest is about 10,000 in./sec. Gas guns have been quite useful for cylindrical projectiles of about 0.5-in. diameter in this velocity range[2]; a modified design to reduce the scatter in velocity from shot to shot and increase the ease of operation was used in this study[3,12]. With this gun it is possible to repeat the velocity of 0.5-in.-diam projectiles weighing between 0.01 lb and 0.50 lb to ± 0.5 percent for velocities in the range 500 to 10,000 in./sec.

The most convenient parameter of the plate response to measure is the transverse displacement, velocity or acceleration. A transducer can only make a measurement at one point and its mass may influence the local behavior at high accelerations. These problems and the short times involved make some kind of photographic technique attractive. The moiré image formed between a set of parallel straight lines and their shadows on a matte surface can be interpreted as a set of level contours under the proper conditions[13,14]. From Fig. 1 it can be seen that differences in elevation between fringes are:

$$h = \frac{p}{\tan\theta_1 + \tan\theta_2} \qquad (1)$$

where p = the pitch of the moiré grid
θ_1 = angle of incidence of the light
θ_2 = viewing angle.

The incident light need not be coherent but must be highly collimated to keep from losing contrast as the distance between grid and surface increases.

Since the plate has a transverse velocity, the luminosity of a point is changing in time; the combination of this with penumbra effects means that the effective exposure time must be limited to maintain sufficient contrast[11]. In this case, a fringe constant of 0.036 in., an impact velocity of 3600 in./sec and a light distance of 20 ft with an 8-in. reflector meant that the exposure time should be kept below about 5 μsec.

Still Camera

The first photographic method used was to take single-frame pictures with a single flash at a calibrated time delay after impact. A set of typical pictures at different time delays after impact are shown in Fig. 2. In this case, the projectile was a blunt cylinder, 0.486-in. diameter, weighing 14.7 gm and traveling at 3600 ± 30 in./sec. Four of the six frames in the composite photograph show the shape of a 0.100-in. thick, 2024-T3 aluminum plate at the specified times after impact. One of the frames shows the resultant static shape after elastic recovery. The sixth frame is a calibration photograph of a truncated cone with a slope of 0.2 used for calibration of the fringe constant.

The two lines of discontinuity, horizontal and vertical, are in the moiré which was made by printing a smaller moiré master four times on the acrylic sheet. A careful examination of the calibration photograph will show that the fringe constant varies in the horizontal direction as a function of radius. This is caused by the effective observation angle of the 8-in. focal-length lens used; the effective spacing of 0.7 in. makes the total radius 8.7 in. For radial distances in the plane of the light beam from +1 in. to −1 in., the denominator of eq (1) changes from 1.10 to 0.90. The additional correction due to displacement change[13] is negligible in comparison with this. In this range, the fringe constant h varies almost linearly with distance; the zero reading on the flat plate was set to a constant illuminance by tilting the moiré grid while observing the fringes on a ground-glass back on the camera. After correcting for this anisotropy in calibration, the deflection was axisymmetric in

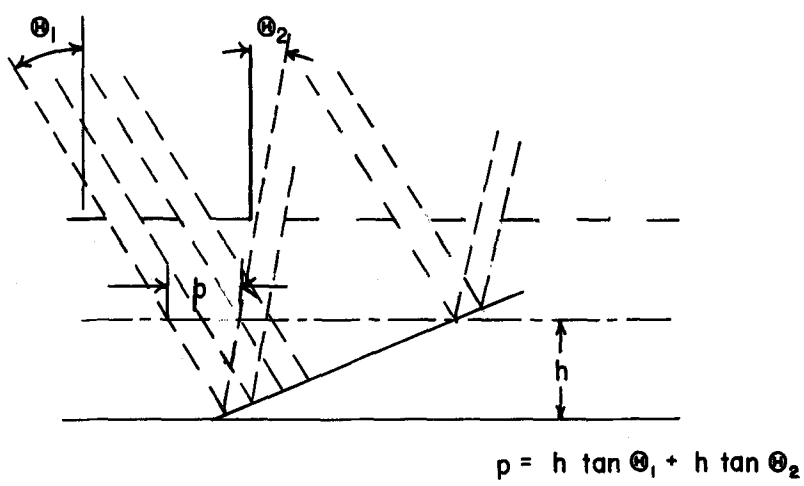

Fig. 1—Geometry of moiré shadow fringes

spite of 10 to 20-percent anisotropy in yield stress between the rolling and transverse directions on the plate.

Streak Camera

A number of preliminary measurements were made with the still camera. The problems with determining contact time and fringe zero gave more scatter in the measured displacements as a function of time than could be tolerated. As a result, a streak camera was developed to show the moiré fringes along a single radial line as a function of time. The detailed design will be reported elsewhere but the general principles are presented here to explain the results.

Our camera is built around a turret with a prismatic surface whose plan is a regular polygon of 66 faces (Fig. 3). A front-silvered mirror is glued to each face. The single lens is an anastigmatic photographic objective with a focal length of 24 in. and a diameter of 3.5 in. (f/16.9). The film plane is placed 24 in. from the plane of the lens and parallel to it as shown. By means of a stationary mirror a plane midway between the viewing slit with the moiré grid and the specimen is also placed 24 in. from the lens. The light from an electronic flash at a distance of 20 ft is reflected through two stationary mirrors to fall on the specimen through another part of the moiré grid at an angle of 45 deg. The light reflected from the matte surface of the specimen forms parallel rays between the lens and the turret. It is reflected back by one of the turret

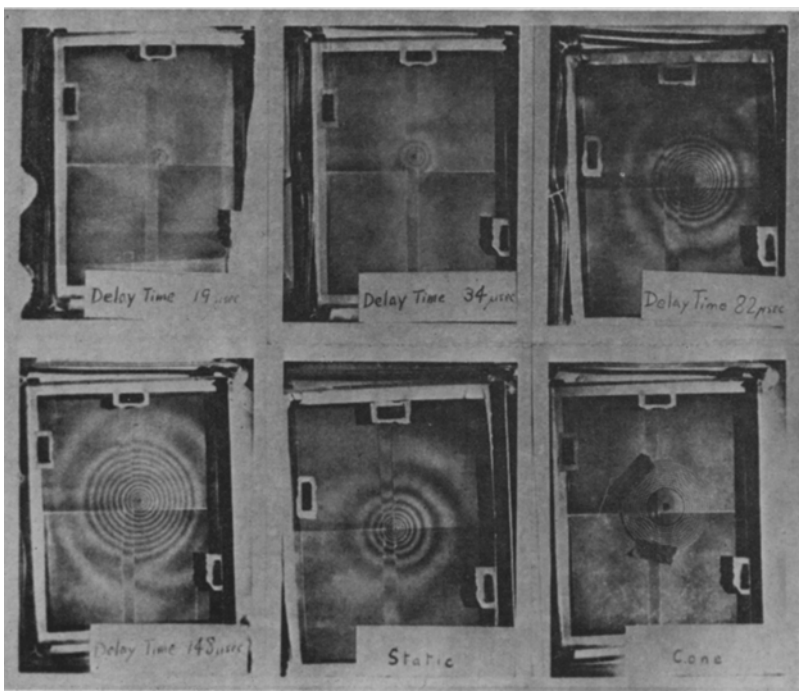

Fig. 2—Still-camera moiré fringes at various times after impact

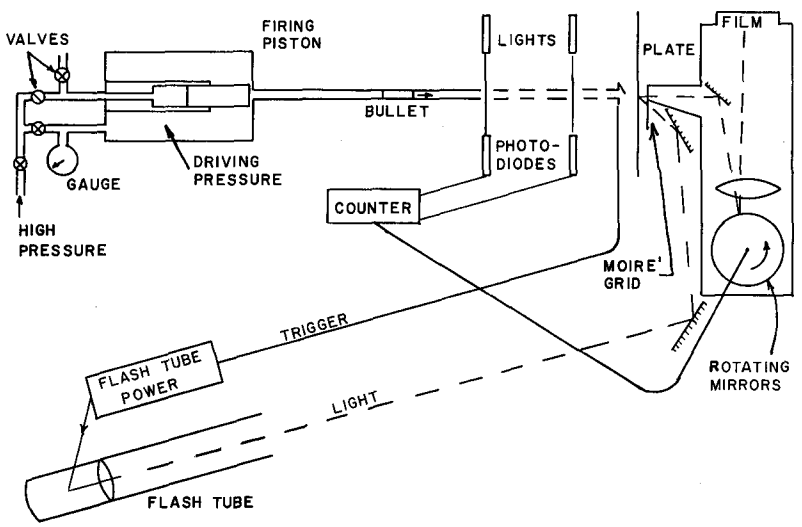

Fig. 3—Experimental arrangement including streak camera

mirrors again as parallel rays to be refocussed on the film. The film length, 4.5 in., is such that one image of the slit is on the film at all times, one entering from the left as one leaves to the right.

At 200 μsec to cover 4.5 in. on the film, a slit width of 0.09 in. gives an exposure time of 4 μsec. There is a slight variation in the fringe constant due to the change in viewing angle as the mirror moves past the back of the lens. The fringe constant was determined by placing a wedge with a slope of 0.2 in front of the moiré slit and then sweeping this stationary image across the film. The measured and the calculated variation are both 3.6 percent. The rotational velocity of the turret is adjusted to avoid double exposure on the film while using the full width. The only drawback to this random-access technique is that the start of the light pulse can occur at any point on the film which means that two different mirrors contribute the beginning and the end of the record and registration is not precise. A typical streak photograph with similar parameters as Fig. 2 is shown in Fig. 4. Unavoidably, there is an uncertainty of something less than half a fringe because the point of minimum intensity is unknown. In this photograph, originally 3.5 × 4.5 in., the impact point is about 0.5 in. from the bottom, the image slit runs vertically and time increases from right to left. Using calibration data appropriate to the lateral location, displacements corresponding to full and half fringes (light and dark lines) are plotted for selected times after impact in Fig. 5. Zero time is judged by the just noticeable change in light intensity at the impact point.

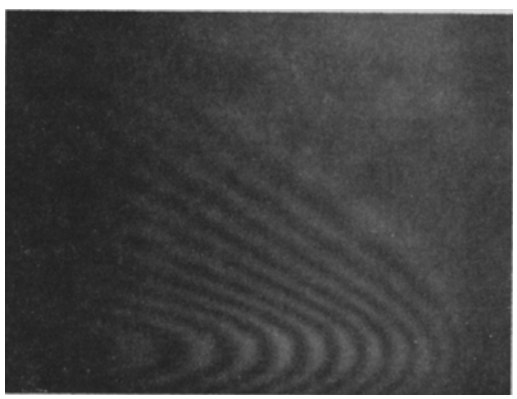

Fig. 4—Streak photograph. 47-gm projectile, 2865-in./sec impact velocity, 300-μsec sweeptime, 3.5-in. slit length

Photomultiplier Measurements

The exact time for individual fringe orders at the point of impact is difficult to determine from the streak photograph because of fringe broadening. To supplement the streak data, a photomultiplier tube was used on the ground-glass screen of the still camera to count the fringe order as a function of time. A typical displacement curve as a function of time for similar parameters as before is shown in Fig. 6. Curves such as these were used to verify the displacements at the edge of the impact area in the curves similar to those of Fig. 5.

Analysis

Assumptions and Approximations

The transverse dynamic equation for the axisymmetric motion of a thin plate is [15]:

$$\frac{1}{r}\frac{\partial}{\partial r}\left[r\frac{\partial M_r}{\partial r} + M_r - M_\theta + rN_r\frac{\partial w}{\partial r}\right] = 2b\,\rho\frac{\partial^2 w}{\partial t^2} \quad (2)$$

where M_θ = bending moment on circumferential surface
M_r = bending moment on radial plane
N_r = in-plane radial-force intensity
w = transverse displacement
$2b$ = thickness of plate
ρ = density
t = time

For full yielding in bending, the maximum value of M_r is Yb^2 and for full yielding in tension, the maximum value of N_r is $2Yb$, where Y is the yield stress. Measurements such as those in Fig. 5 show slopes of 0.1 to 0.2. For these slopes, the term involving N_r in

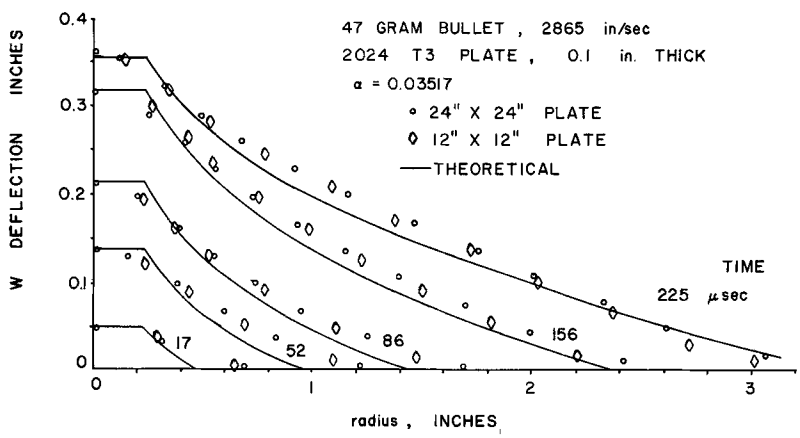

Fig. 5—Comparison of measured and predicted displacement vs. radius for five selected times and two plate sizes, 2024T3 alloy

eq (6) dominates those involving bending moment unless the moment changes from its maximum to zero in less than two and one half times the plate thickness. This can be used in assessing the relative importance of shear, the derivative of bending moment, and membrane forces in the regions of relatively large slope. In this work, we assume that there are four regions in the plate. The first region is the elastic portion of the plate at radii beyond that reached by the shear wave:

$$r_s = c_s t + r_M \tag{3}$$

where

r_M = radius of blunt projectile

and

$$c_s = \sqrt{G/\rho}$$

Beyond this radius there is a compressive wave which causes no transverse deflection. Inside this radius there is elastic bending until the slope becomes large enough to cause membrane stresses of significant size. It will be shown in the next section that r_b, the radius beyond which the elastic-bending solution holds, is given by:

$$r_b = c_M t + r_M \tag{4}$$

where

$$c_M = \sqrt{Y/\rho}$$

Inside this radius is a region where the plate deformation is governed almost completely by membrane force; not only is the bending moment small because of yield interaction with the slope-induced radial tension but its effect is even smaller because its variation is small [eq (2)]. The fourth region is that inside the radius of the bullet which travels at the current bullet velocity. To make the analysis simpler, and because it gives reasonable results, we have made the assumption that the plate has yielded through the thickness and that there is a constant membrane stress equal to the yield stress in the radial direction in the membrane region. This result is basically different from that found by Clark, Duwez, and Bohnenblust[4] for the beam since the beam has no tangential constraint to cause membrane stress.

Governing Equations

With the assumptions of the previous section, eq (2) becomes

$$\frac{1}{r}\frac{\partial}{\partial r}\left(r\frac{\partial w}{\partial r}\right) - c_M{}^2\frac{\partial^2 w}{\partial t^2} = 0 \tag{5}$$

The boundary condition at large radii is:

$$\left.\begin{aligned} w\,(r,t) &= 0 \\ \frac{\partial w}{\partial t}\,(r,t) &= 0 \end{aligned}\right\} r > r_b \tag{6}$$

This is not exact since there are elastic bending waves outboard of r_b but for the range of parameters studied in this project, the displacements and velocities in the elastic region are negligible in comparison with those in the plastic region. For very thick plates or for those with low yield stress and, thus, a low membrane wave velocity, some modification of this boundary condition will have to be made. The other boundary condition is at the edge of the impact area of the projectile where the acceleration of the total mass is caused by the membrane force acting on the slope of the plate at this radius:

$$2\pi r_M\, Y2b\frac{\partial w}{\partial r} = (M+\Delta M)\frac{\partial^2 w}{\partial t^2} \text{ at } r = r_M \tag{7}$$

where r_M = radius of projectile
M = mass of projectile
$\Delta M = \pi r^2 2b\,\rho$

This can be put in convenient form for computation by letting

$$\left.\begin{aligned} \bar{r} &= r/r_M \\ \bar{t} &= ct/r_M \end{aligned}\right\} \tag{8}$$

Then eq (5) becomes:

$$\frac{\partial^2 w}{\partial \bar{r}^2} + \frac{1}{\bar{r}}\frac{\partial w}{\partial \bar{r}} - \frac{\partial^2 w}{\partial \bar{t}^2} = 0 \tag{9}$$

with the boundary and initial conditions:

$$\left.\begin{aligned} \alpha\frac{w}{\bar{r}} &= \frac{\partial^2 w}{\partial \bar{t}^2} && \bar{r} = 1\ t \geq 0 \\ w\,(\bar{r},0) &= 0 && \bar{r} \geq 1 \\ \frac{\partial w}{\partial t}\,(\bar{r},0) &= \begin{cases} \bar{v}_o & \bar{r} = 1 \\ 0 & \bar{r} > 1 \end{cases} \end{aligned}\right\} \tag{10}$$

where

$$\alpha = \frac{2\Delta M}{M + M}$$

$$\bar{V}_o = V_o\frac{M}{M+\Delta M}\frac{r_M}{c}$$

V_o = impact velocity of the projectile

The solution to these equations is directly proportional to $\bar{V}_o$ so that:

$$w = \bar{V}_o\,\varphi\,(\bar{r},\bar{t};\alpha) \tag{11}$$

The function φ for a range of values of α was calculated numerically by two different methods whose results agreed quite well[11]. The first technique was to take the Laplace transform of the field equation and the boundary condition. The transformed field equation is Bessel's equation and can be solved explicitly so as to satisfy the boundary conditions. The inverse can now be found by a contour integral which can be evaluated numerically. A more practical method is to use finite-difference approximations for the derivatives with respect to r and t. If we let $\Delta r = c_M \Delta t$ or $\Delta \bar{r} = \Delta \bar{t}$, this is equivalent to integrating along the characteristics and gives remarkably small round-off error[16].

Comparison Between Measured and Computed Displacements

Time History of Impact Point

Displacement measurements of the impact point as a function of time were taken using the photomultiplier tube for many combinations of plate thickness from 0.025 in. to 0.19 in., projectile masses

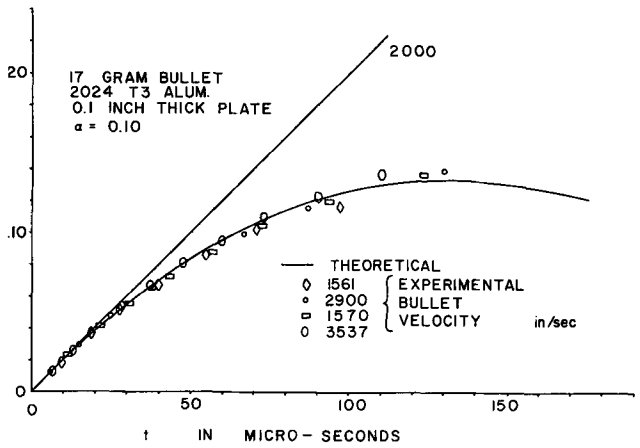

Fig. 6—Comparison of measured and predicted displacement vs. time for various velocities

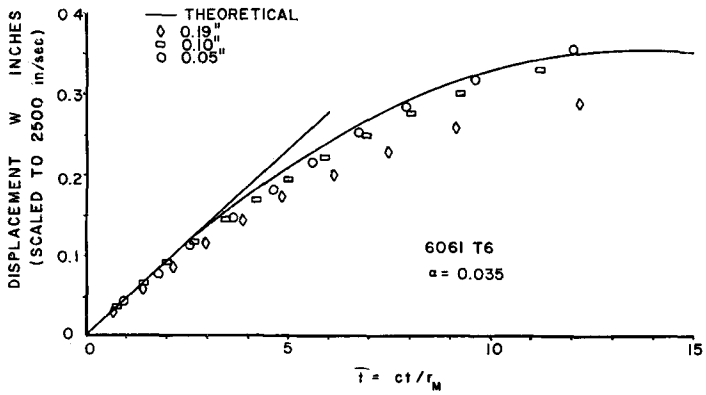

Fig. 7—Comparison of measured and predicted displacement vs. time for different plate thicknesses

from 15 gms to 100 gms, impact velocities between 1000 and 4000 in./sec and for three different aluminum alloys. The alloys used were 2024T3, 6061T6 and 7075T6. In our calculations, we used average values of yield stress of 50,000 psi, 40,000 psi and 70,000 psi for them, respectively; test coupons showed some variation in yield stress between the rolling and transverse directions, but these seemed to be good average values. Figure 6 shows deflection of a 0.100-in.-thick 2024T3 plate as a function of time for a range of impact velocities with the displacement scaled by the ratio of 2000 in./sec to the measured velocity. The predicted curve was found from eqs (11) and (12) using numerical integration on the finite-difference approximation and an α of 0.035. Figure 7 shows similar data for three thicknesses of 6061T6 plate. In these cases, the bullet masses were changed in the ratios of the plate thicknesses to keep $\alpha = 0.035$. As the plate thickness becomes comparable to the maximum deflection, the bending effects become more important and the deflections are less than would be predicted by the simple-membrane theory.

Deformation Shape

Figure 5 shows deflection as a function of radius for five times for two different plate sizes. The repeatability is typical of that for all tests. Since there did not appear to be any difference in the results between 12-in.-square and 2-in.-square plates, most measurements were made with the smaller size. Since the reflected waves had no influence on the initial time history up to the point of maximum displacement, the plates were supported in the most convenient fashion; the edges rested against angles which prevented the whole plate from being displaced far enough to hit the camera. A simple momentless support, almost but not quite rigid, is a reasonable approximation to the actual condition.

Figures 8 and 9 show displacement, scaled to 2500-in./sec impact velocity, vs. dimensionless radius for three dimensionless times. Each figure is

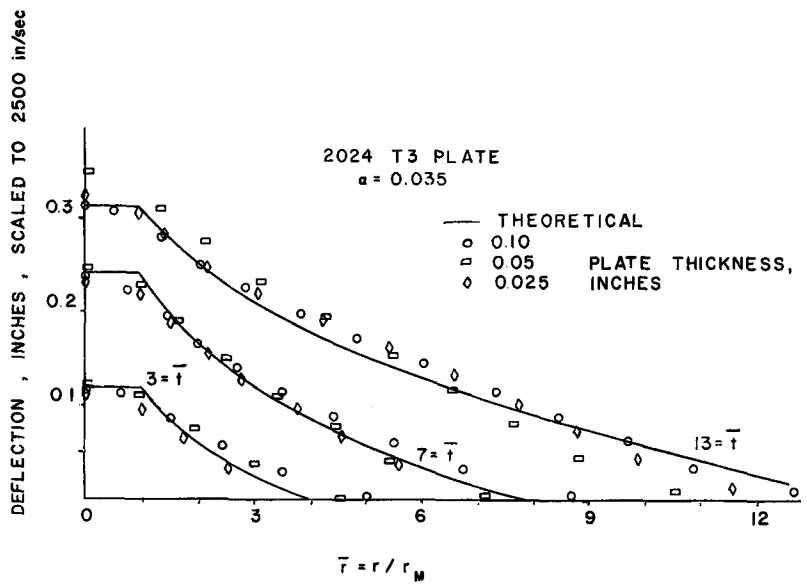

Fig. 8—Comparison of measured and predicted displacement vs. radius for five selected times and three plate thicknesses, 2024T3 alloy

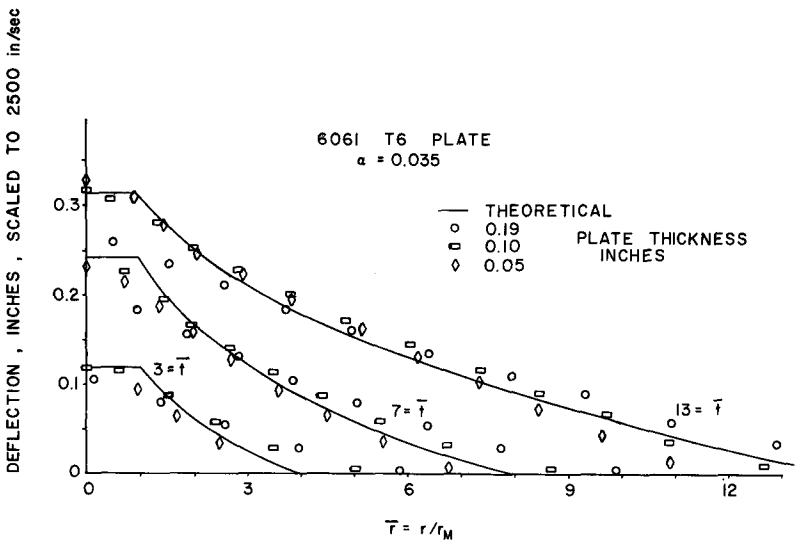

Fig. 9—Comparison of measured and predicted displacement vs. radius for five selected times and three plate thicknesses, 6061T6 alloy

for a different alloy and each shows experimental results for three plate thicknesses. The mass of the projectile was scaled to the plate thickness so that $\alpha = 0.035$. The reduction in deflection for large plate thicknesses noted before in Fig. 7 can be seen to occur only for small radii in Fig. 9. The relative retardation of the zero displacement associated with the elastic bending wave at large times is stronger for thin plates. This is probably because the bending-wave velocity is proportional to the square root of the plate thickness. The experimental results for the 0.025-in.-thick plate in Fig. 8 do not seem to follow the trend for the thicker plates in Figs. 8 and 9.

Conclusions

For thin plates under transverse impact, the dynamic plastic deformation is governed by membrane stress. To a first approximation, it can be assumed that the radial deformation and tangential strain of the middle surface is negligible. The radial strain is relatively small, amounting only to several times the elastic strain at nominal yield; this means that a small-strain, large-deflection theory is applicable. A deformation theory based on a constant membrane stress in the radial direction equal to the yield stress in tension adequately predicts the time history during plastic deformation up to first arrest of the projectile; this all takes place within several hundred microseconds. While such a simplified analysis is adequate for dynamics and deformations, it cannot predict the details of the stress–strain trajectory.

As always, this investigation has left open a number of intriguing questions. Among these are: what is the interaction with bending stress in thick plates; what is the effect of relatively slow elastic bending waves in thin plates; what is the effect of relatively slow membrane waves in low-yield materials; what is the effect of relatively fast membrane waves in high-yield materials? These last two are closely related to the problem of perforation, since it is clear that kinetic energy of impact cannot be absorbed unless it can be transmitted to the plate material; this, in turn, cannot be done before perforation unless the wave velocity is high. Thus one should expect perforation at a lower velocity for a low-yield-strength material, but only the radial yield stress has much influence.

Acknowledgment

This work was supported by the Air Force Materials laboratory under the supervision of T. Nicholas and J. P. Henderson. Permission to publish is gratefully acknowledged.

References

1. *Goldsmith, W., Impact, Edward Arnold Ltd., London (1960).*
2. *Goldsmith, W., Liu, T. W. and Chulay, S., "Plate Impact and Perforation by Projectiles,"* EXPERIMENTAL MECHANICS, *5 (12), 385-404 (Dec. 1965).*
3. *Yamaishi, K., "Elastic Behavior of Aluminum Plates Under Transverse Bullet Impact," Masters Thesis, University of Minnesota (June 1969).*
4. *Duwez, P. E., Clark, D. S. and Bohnenblust, H. F., "The Behavior of Long Beams Under Impact Loading," Jnl. Appl. Mech., 17 (1), 27-34 (1950).*
5. *a) Hopkins, H. G. and Prager, W., "On the Dynamics of Circular Plates," Z.A.M.P., 5, 317-331 (July 1954). b) Wang, A. J. and Hopkins, H. G., "On the Plastic Deformation of Built-In Circular Plates Under Impulsive Load," Jnl. Mech. Phys. of Solids, 3, 22-37 (1954).*
6. *Galin, M. P., "Impact of Flexible Plates," Sborn. Stat. Inst. Mech., Acad. Nauk. SSSR (1949).*
7. *Rakhmatulin, K. H. and Demyanov, Y. U., Strength Under High Transient Loads, Daniel Daney, New York, 206-240 (1966).*
8. *Dinca, G., "Deformari Rapide Ale Membranelor Extensible," St. Cerc. Mat., 77 (5), Bucharest, 817-825 (1965).*
9. *Cristescu, N., Dynamic Plasticity, North Holland Publ. Co., Amsterdam (1967).*
10. *Duffey, T. A. and Key, S. W., "Experimental Theoretical Correlations of Impulsively Loaded Clamped Circular Plates,"* EXPERIMENTAL MECHANICS, *9 (6), 241-249 (June 1969).*
11. *Beynet, P., "Plastic Plate Impact Without Perforation," Ph.D. Thesis, University of Minnesota (1970).*
12. *Plunkett, R., Godfrey, D. E., Yamaishi, K. and Beynet, P., "A Gas Gun for Transonic Velocities," AFML-TR-69-345 (1969).*
13. *Hazell, C. R., "Visualization of Lateral Displacements of Vibrating Plates by the Shadow Moire Method," Jnl. Mech. Eng. Sci., 2 (2), 214-219 (1969).*
14. *Theocaris, P. S., "Moire Fringes: A Powerful Measuring Device," Appl. Mech. Surveys, H. N. Abramson et. al. ed. Spartan Books, Washington, D. C., 613-626 (1966).*
15. *Timoshenko, S., Theory of Plates and Shells, McGraw-Hill, New York (1940).*
16. *Crandall, S. H., Engineering Analysis, McGraw-Hill, New York, Sec. 6-5 (1956).*